INTERNATIONAL JOURNAL FOR NUMERICAL METHODS IN FLUIDS
Int. J. Numer. Meth. Fluids 2008; **58**:1041–1062
Published online 20 March 2008 in Wiley InterScience (www.interscience.wiley.com). DOI: 10.1002/fld.1785

Hybrid and multi-point formulations of the lowest-order mixed methods for Darcy's flow on triangles

Anis Younes[1,*,†] and Vincent Fontaine[2]

[1]*Institut de Mécanique des Fluides et des Solides, Université Louis Pasteur de Strasbourg-CNRS/UMR 7507, 2 rue Boussingault, F-67000 Strasbourg, France*
[2]*Laboratoire de Physique des Bâtiments et des Systèmes, Université de la Réunion, 15 avenue René Cassin, BP 7151-97715 Saint-Denis Cedex 09 La Réunion, France*

SUMMARY

Mixed finite element (MFE) and multipoint flux approximation (MPFA) methods have similar properties and are well suited for the resolution of Darcy's flow on anisotropic and heterogeneous domains.

In this work, the link between hybrid and MPFA formulations is shown algebraically for the lowest order mixed methods of Raviart–Thomas (RT0) and Brezzi–Douglas–Marini (BDM1) on triangles. The efficiency of the four mixed formulations (Hybrid_RT0, MPFA_RT0, Hybrid_BDM1 and MPFA_BDM1) is investigated on high anisotropic and heterogeneous media and for unstructured triangular discretizations.

Numerical experiments show that the MPFA_BDM1 formulation outperforms both Hybrid_RT0 and Hybrid_BDM1 in the case of anisotropic domains and highly unstructured meshes. Copyright © 2008 John Wiley & Sons, Ltd.

Received 1 July 2007; Revised 14 January 2008; Accepted 17 January 2008

KEY WORDS: mixed method; Raviart–Thomas space; Brezzi–Douglas–Marini space; hybrid formulation; multipoint flux approximation

1. INTRODUCTION

We consider the numerical solution of the following partial differential equation (PDE):

$$\begin{aligned} \nabla(-\mathbf{K}\nabla p) &= f \quad && \text{in } \Omega \\ P &= P_e \quad && \text{on } \partial\Omega_{\mathrm{D}} \\ -K\frac{\partial P}{\partial \eta} &= g \quad && \text{on } \partial\Omega_{\mathrm{N}} \end{aligned} \tag{1}$$

*Correspondence to: Anis Younes, Institut de Mécanique des Fluides et des Solides, Université Louis Pasteur de Strasbourg-CNRS/UMR 7507, 2 rue Boussingault, F-67000 Strasbourg, France.
†E-mail: younes@imfs.u-strasbg.fr

where Ω is a bounded polygonal open set of $\mathbb{R}^2$, $\partial\Omega_D$ and $\partial\Omega_N$ are partitions of the boundary $\partial\Omega$ of Ω corresponding to Dirichlet and Neumann conditions and η the unit outward vector normal to the boundary $\partial\Omega$.

The PDE (1) is a very common mathematical model in physics used to simulate steady-state diffusion processes such as heat or mass transfer or flow in porous media.

In the context of flow in porous media, considered in this paper, the state variable p corresponds to the pressure or the piezometric head, $\mathbf{K}$ is a symmetric positive-definite permeability tensor and f the sink/source term.

The mixed finite element (MFE) method is well suited for the discretization of (1) since it is locally conservative and handles general irregular grids with anisotropic and heterogeneous permeability [1].

The MFE method uses both the velocity and the pressure as primary unknowns. To this aim, Darcy's velocity $\mathbf{q}$ is introduced as an additional unknown and PDE (1) is transformed to the following system:

$$\begin{aligned} \mathbf{q} &= -\mathbf{K}\nabla p \\ \nabla\mathbf{q} &= f \end{aligned} \tag{2}$$

Mixed methods have been extensively employed during the past few years ([1–9], among others). For practical applications, lowest-order mixed methods of Raviart–Thomas (RT0) or Brezzi–Douglas–Marini (BDM1) are usually used and will be considered in the current paper. Both RT0 and BDM1 use a piecewise constant approximation for the pressure [3]. The velocity space has three degrees of freedom with RT0 and six with BDM1.

In their original form, the mixed methods require the resolution of systems of algebraic equations that are typically indefinite [3, 10]. This problem is generally circumvented by hybridization [11], which is the most widely used approach. System (2) is solved in this case for the pressure Lagrange multipliers at element edges.

Many authors tried to reduce the number of unknowns for RT0 and to find the link with the standard finite volume method. For rectangular meshes, the RT0 mixed method can be reduced to the standard cell-centred finite volume method, when numerical integration with quadrature rules is used [12, 13]. This procedure was extended to triangular meshes [14, 15], but the diagonalization of the elemental matrix by numerical quadrature appears to be an accurate approximation only if triangles have three sharp angles. Reduction to one unknown per element without any numerical integration has been obtained in [6, 8, 16] for triangular elements.

Recently, mixed methods were related to a new finite volume method called multipoint flux approximation (MPFA) method. The MPFA discretization is a control volume formulation where more than two pressure values are used in the flux approximation [17–20]. Indeed, it was shown in [21] that the RT0 MFE method is equivalent to a particular non-symmetric MPFA method, and this without any numerical integration. On the other hand, the use of a specific quadrature rule with BDM1 method allows for local flux elimination and can be shown to be equivalent to a symmetric MPFA method [22–26].

In this paper, we show algebraically the link between hybrid and MPFA formulations of both RT0 and BDM1 methods on triangular meshes. These meshes are suitable for practical problems with complex geometry and local mesh refinement. The efficiency and accuracy of the four mixed formulations (Hybrid_RT0, MPFA_RT0, Hybrid_BDM1 and MPFA_BDM1) are investigated on high anisotropic and heterogeneous media and with unstructured triangular discretizations.

DOI: 10.1002/fld

2. THE HYBRID FORMULATION OF RT0 AND BDM1

The idea of hybridization goes back to Fraeijs de Veubeke [27]. The assumption that the velocity is continuous across elements boundary is dropped. New variables corresponding to the pressure at edges, assumed to be constant for RT0 and linear for BDM1, are defined and viewed as Lagrange multiplier. The velocity space can then be eliminated at the element level, and an extra equation is added to ensure continuity of the normal component of the velocity. The principal stages of the hybrid formulation of RT0 and BDM1 are summarized in this section.

2.1. Approximation spaces

Let us consider the triangular element A with three edges A_i and let $\widehat{A}$ denote the reference triangle with vertices $(0,0)$, $(1,0)$ and $(0,1)$.

The solution of the system (2) is approximated over A by $P^A \in \mathbb{R}$, the constant value of P over the element A. The velocity $\mathbf{q}$ over A is approximated by $\mathbf{q}_A \in \mathbf{X}_A$, where $\mathbf{X}_A$ is the RT0 or the BDM1 space [1, 28].

With RT0, $\mathbf{q}_A$ may be expressed as

$$\mathbf{q}_A = \sum_{i=1}^{3} Q_i^A \boldsymbol{\omega}_i^{\mathrm{RT0}} \tag{3}$$

The normal component of the velocity, $\mathbf{q}_A \cdot \mathbf{n}_{A_i}$, is constant over the edge A_i. The velocity inside the element has three degrees of freedom: one degree of freedom per edge (see Figure 1).

The expressions of the vectorial basis functions, in the reference element, are given in Table I and obtained from

$$\widehat{\boldsymbol{\omega}}_i^{\mathrm{RT0}} = \begin{pmatrix} a_i^{\mathrm{RT0}} + b_i^{\mathrm{RT0}} \hat{x} \\ c_i^{\mathrm{RT0}} + b_i^{\mathrm{RT0}} \hat{y} \end{pmatrix} \quad \text{for } i = 1, \ldots, 3 \tag{4}$$

where $\widehat{x}, \widehat{y}$ are coordinates on the reference element.

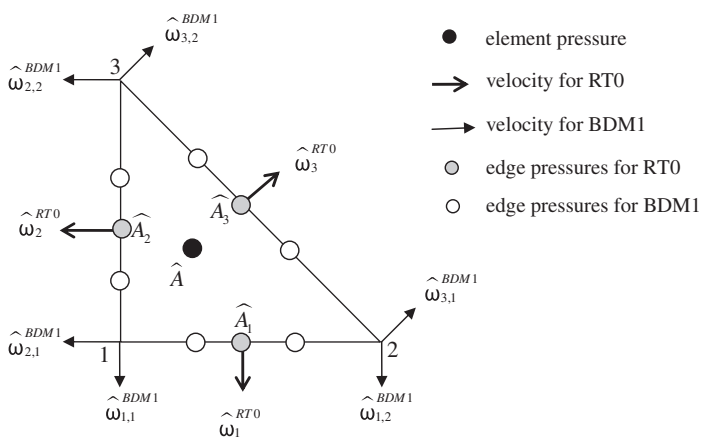

Figure 1. Degrees of freedom and basis functions for RT0 and BDM1 spaces on triangles.

DOI: 10.1002/fld

Table I. Vectorial basis functions for RT0 and BDM1 in the reference element.

	RT0	BDM1
Edge 1	$\widehat{\boldsymbol{\omega}}_1^{\mathrm{RT0}}=(\hat{x},\hat{y}-1)^{\mathrm{T}}$	$\widehat{\boldsymbol{\omega}}_{1,1}^{\mathrm{BDM1}}=2(0,\hat{x}+\hat{y}-1)^{\mathrm{T}}$, $\widehat{\boldsymbol{\omega}}_{1,2}^{\mathrm{BDM1}}=2(\hat{x},-\hat{x})^{\mathrm{T}}$
Edge 2	$\widehat{\boldsymbol{\omega}}_2^{\mathrm{RT0}}=(\hat{x}-1,\hat{y})^{\mathrm{T}}$	$\widehat{\boldsymbol{\omega}}_{2,1}^{\mathrm{BDM3}}=2(\hat{x}+\hat{y}-1,0)^{\mathrm{T}}$, $\widehat{\boldsymbol{\omega}}_{2,2}^{\mathrm{BDM1}}=2(-\hat{y},\hat{y})^{\mathrm{T}}$
Edge 3	$\widehat{\boldsymbol{\omega}}_3^{\mathrm{RT0}}=(\hat{x},\hat{y})^{\mathrm{T}}$	$\widehat{\boldsymbol{\omega}}_{3,1}^{\mathrm{BDM1}}=2(\hat{x},0)^{\mathrm{T}}$, $\widehat{\boldsymbol{\omega}}_{3,2}^{\mathrm{BDM1}}=2(0,\hat{y})^{\mathrm{T}}$

On the edge A_l, we set

$$\int_{A_l}\widehat{\boldsymbol{\omega}}_i^{\mathrm{RT0}}\mathbf{n}_{A_l}=\delta_{il}\quad\text{for } l=1,\ldots,3 \tag{5}$$

Hence,

$$\int_A\nabla\boldsymbol{\omega}_i^{\mathrm{RT0}}=\int_{\widehat{A}}\nabla\widehat{\boldsymbol{\omega}}_i^{\mathrm{RT0}}=1\quad\text{for } i=1,\ldots,3 \tag{6}$$

with BDM1, $\mathbf{q}_A$ may be expressed as

$$\mathbf{q}_A=\sum_{i=1}^{3}\sum_{j=1}^{2}Q_{i,j}^{A}\boldsymbol{\omega}_{i,j}^{\mathrm{BDM1}} \tag{7}$$

The normal component of the velocity is linear on each edge. The velocity inside the element has six degrees of freedom: two degrees of freedom per edge (see Figure 1).

In this work, the degrees of freedom on each edge are associated with the values of $\mathbf{q}_A\cdot\mathbf{n}_{A_i}$ at the vertices of the edge A_i as in [24, 29]. This choice guarantees certain orthogonalities for the quadrature rule (introduced later in Section 4.2).

The expressions of the vectorial basis functions, in the reference element, are given in Table I and obtained from

$$\widehat{\boldsymbol{\omega}}_{i,j}^{\mathrm{BDM1}}=\begin{pmatrix}a_{i,j}^{\mathrm{BDM1}}+b_{i,j}^{\mathrm{BDM1}}\hat{x}+c_{i,j}^{\mathrm{BDM1}}\hat{y}\\ d_{i,j}^{\mathrm{BDM1}}+e_{i,j}^{\mathrm{BDM1}}\hat{x}+f_{i,j}^{\mathrm{BDM1}}\hat{y}\end{pmatrix}\quad\text{for } i=1,\ldots,3 \text{ and } j=1,\ldots,2 \tag{8}$$

and by setting, on the edge A_l with the two end points (vertices) $\mathbf{r}_{lk}(k=1,2)$,

$$\widehat{\boldsymbol{\omega}}_{i,j}^{\mathrm{BDM1}}(\mathbf{r}_{lk})\mathbf{n}_{A_l}=2\delta_{il}\delta_{jk}\quad\text{for } l=1,\ldots,3 \text{ and } k=1,2 \tag{9}$$

Hence,

$$\int_A\nabla\boldsymbol{\omega}_{i,j}^{\mathrm{BDM1}}=\int_{\widehat{A}}\nabla\widehat{\boldsymbol{\omega}}_{i,j}^{\mathrm{BDM1}}=1\quad\text{for } i=1,\ldots,3 \text{ and } j=1,\ldots,2 \tag{10}$$

With the hybrid formulation of MFE, the continuity of the normal component is forced via the Lagrange multiplier, which is viewed as the pressure on the edge. This edge pressure is assumed to be constant, with one degree of freedom corresponding to TP_i, the mean value of the pressure on the edge A_i, for RT0. For BDM1, the edge pressure is linear, with two degrees of freedom corresponding to $TP_{i,1}$ and $TP_{i,2}$, the edge pressure values at two points on edge A_i.

DOI: 10.1002/fld

2.2. Discretization with RT0

The variational formulation of Darcy's law ($\mathbf{K}^{-1}\mathbf{q}=-\nabla p$) is expressed using the vectorial basis functions $\boldsymbol{\omega}_i^{\mathrm{RT0}}$ as test functions:

$$\int_A \mathbf{K}^{-1}\mathbf{q}_A\boldsymbol{\omega}_i^{\mathrm{RT0}} = -\int_A \nabla P\boldsymbol{\omega}_i^{\mathrm{RT0}} = \int_A P\nabla\boldsymbol{\omega}_i^{\mathrm{RT0}} - \sum_{k=1}^{3}\int_{A_k} P\boldsymbol{\omega}_i^{\mathrm{RT0}}\mathbf{n}_k \tag{11}$$

Using (5) and (6), we obtain

$$\int_A \mathbf{K}^{-1}\mathbf{q}_A\boldsymbol{\omega}_i^{\mathrm{RT0}} = P^A - TP_i^A \tag{12}$$

Using (3), (12) can be expressed in the following matrix form:

$$\sum_{k=1}^{3} B_{i,k}Q_k^A = P^A - TP_i^A \tag{13}$$

where the elemental matrix $B=[B_{i,k}]$ of dimensions (3×3) is defined by

$$B_{i,k} = \int_A \boldsymbol{\omega}_i^{\mathrm{RT0,T}}\mathbf{K}^{-1}\boldsymbol{\omega}_k^{\mathrm{RT0}} \tag{14}$$

This matrix can be evaluated analytically in the reference element using

$$B_{i,k} = \int_A \widehat{\boldsymbol{\omega}}_i^{\mathrm{RT0,T}}\widehat{\mathbf{K}}^{-1}\widehat{\boldsymbol{\omega}}_k^{\mathrm{RT0}} \tag{15}$$

where $\widehat{K}^{-1}=J^{\mathrm{T}}K^{-1}J/|J|$ corresponds to the analog tensor in the reference element, and J is Jacobian matrix that is constant for triangular elements.

The matrix B is symmetric and positive definite. Equation (13) can be expressed as

$$Q_i^A = \sum_{k=1}^{3} B_{i,k}^{-1}(P^A - TP_k^A) \tag{16}$$

The mass balance equation in (2) is discretized using a finite volume formulation in space:

$$\sum_{i=1}^{3} Q_i^A = |A|f_A = Q_s^A \tag{17}$$

f_A is the mean value of f over the element A.

Combining (16) and (17) gives

$$P^A = \sum_{i=1}^{3}\frac{\alpha_i}{\alpha}TP_i^A + \frac{Q_s^A}{\alpha} \tag{18}$$

where $\alpha_i=\sum_{k=1}^{3}B_{i,k}^{-1}$ and $\alpha=\sum_{i=1}^{3}\alpha_i$.

Finally, the expression of the flux is given by replacing (18) in (16):

$$Q_i^A = \frac{\alpha_i}{\alpha}\sum_{k=1}^{3}\alpha_k TP_k^A - \sum_{k=1}^{3}B_{i,k}^{-1}TP_k^A + \frac{\alpha_i}{\alpha}Q_s^A \tag{19}$$

DOI: 10.1002/fld

The scalar unknowns with the hybrid formulation of RT0 are the mean pressures on the edges $(TP_i^A, i=1,\ldots,nf)$.

The final system of equations is obtained using continuity properties as follows:

- On all interior edges, continuity of the normal component of the velocity and edge pressure between the two adjacent elements A and B may be expressed as

$$TP_i^A = TP_i^B \quad \text{and} \quad Q_i^A + Q_i^B = 0 \tag{20}$$

- For a Dirichlet boundary edge A_i with a prescribed pressure TP_i^{bc}, we have

$$TP_i^A = TP_i^{bc} \tag{21}$$

- For a Neumann boundary edge with a given flux Q_i^{bc}

$$Q_i^A = Q_i^{bc} \tag{22}$$

The hybrid formulation of RT0 gives a system for the number of edge unknowns with a symmetric positive matrix of a five-point stencil.

2.3. Discretization with BDM1

The variational formulation of Darcy's law ($\mathbf{K}^{-1}\mathbf{q} = -\nabla p$) using the vectorial basis functions $\boldsymbol{\omega}_{i,j}^{\mathrm{BDM1}}$ as test functions may be expressed as

$$\int_A \mathbf{K}^{-1}\mathbf{q}_A \boldsymbol{\omega}_{i,j}^{\mathrm{BDM1}} = -\int_A \nabla P \boldsymbol{\omega}_{i,j}^{\mathrm{BDM1}} = \int_A P \nabla \boldsymbol{\omega}_{i,j}^{\mathrm{BDM1}} - \sum_{k=1}^{3} \int_{A_k} P \boldsymbol{\omega}_{i,j}^{\mathrm{BDM1}} \mathbf{n}_k \tag{23}$$

Setting $TP_{i,1}$ and $TP_{i,2}$ to the edge pressure values at $\frac{1}{3}$ and $\frac{2}{3}$ of the edge and using (7), the previous equation leads to

$$\sum_{k=1}^{3}\sum_{l=1}^{2} Q_{k,l}^A \int_A \boldsymbol{\omega}_{i,j}^{\mathrm{BDM1,T}} \mathbf{K}^{-1} \boldsymbol{\omega}_{k,l}^{\mathrm{BDM1}} = P^A - TP_{i,j}^A \tag{24}$$

The element al matrix $B = [B_{i,j,k,l}]$ is of dimensions (6×6) with

$$B_{i,j,k,l} = \int_A \boldsymbol{\omega}_{i,j}^{\mathrm{BDM1,T}} \mathbf{K}^{-1} \boldsymbol{\omega}_{k,l}^{\mathrm{BDM1}} \tag{25}$$

where B is a positive-definite matrix evaluated analytically in the reference element.

The same calculations as with the RT0 lead to

$$Q_{i,j}^A = \sum_{k=1}^{3}\sum_{l=1}^{2} B_{i,j,k,l}^{-1} (P^A - TP_{k,l}^A) \tag{26}$$

and

$$P^A = \sum_{i=1}^{3}\sum_{j=1}^{2} \frac{\alpha_{i,j}}{\alpha} TP_{i,j}^A + \frac{Q_s^A}{\alpha} \tag{27}$$

where $\alpha_{i,j} = \sum_{k=1}^{3}\sum_{l=1}^{2} B_{i,j,k,l}^{-1}$ and $\alpha = \sum_{i=1}^{3}\sum_{j=1}^{2} \alpha_{i,j}$.

DOI: 10.1002/fld

Replacing (27) in (26) leads to

$$Q_{i,j}^{A}=\frac{\alpha_{i,j}}{\alpha}\sum_{k=1}^{3}\sum_{l=1}^{2}\alpha_{k,l}TP_{k,l}^{A}-\sum_{k=1}^{3}\sum_{l=1}^{2}B_{i,j,k,l}^{-1}TP_{k,l}^{A}+\frac{\alpha_{i,j}}{\alpha}Q_{s}^{A} \tag{28}$$

With this formulation, the scalar unknowns are discrete pressures at edges ($TP_{i,j}^{A}, i=1,\ldots,nf$ and $j=1,\ldots,2$). The final system of equations is obtained using continuity properties as with RT0.

The hybrid formulation of BDM1 leads to a system of twice the number of edge unknowns with a symmetric positive matrix of a 10-point stencil.

3. THE MPFA METHOD ON TRIANGLES

3.1. The MPFA method

The MPFA discretization is a control volume formulation, where more than two pressure values are used in the flux approximation. The scheme reduces to a cell-centred stencil for the pressures [17–20].

The basic idea of the MPFA method is to divide each triangle into four subcells (Figure 2). Inside the subcell $(\mathbf{x}_i, \mathbf{x}_i^2, \bar{\mathbf{x}}, \mathbf{x}_i^1)$ of the corner $\mathbf{x}_i$, we assume linear variation of the pressure between λ_i^1 (the pressure at the midpoint edge $\mathbf{x}_i^1$), λ_i^2 (the pressure at the midpoint edge $\mathbf{x}_i^2$) and P^A (the pressure at the centre $\bar{\mathbf{x}}$ of element A) (Figure 2).

Therefore, subedge (half-edge) fluxes,

$$\left(Q_i^1=\int_{\mathbf{x}_i}^{\mathbf{x}_i^1}-\mathbf{K}\nabla\mathbf{P} \text{ and } Q_i^2=\int_{\mathbf{x}_i}^{\mathbf{x}_i^2}-\mathbf{K}\nabla\mathbf{P}\right)$$

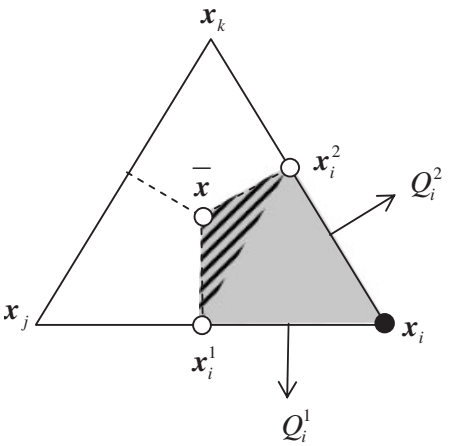

Figure 2. Triangle splitting into four subcells and linear pressure approximation on each subcell.

DOI: 10.1002/fld

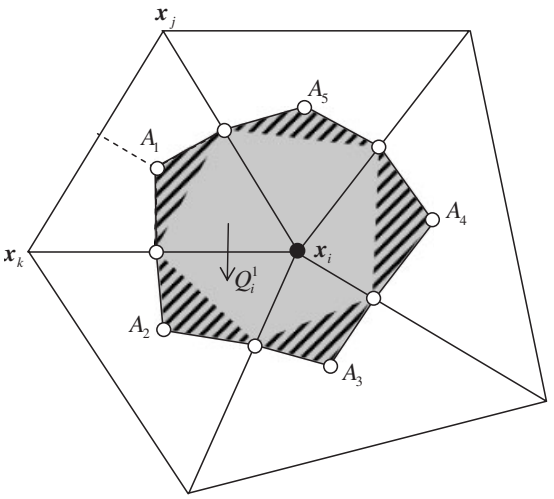

Figure 3. The interaction region sharing vertex i.

taken positive for outflow, are given by

$$\begin{pmatrix} Q_i^1 \\ Q_i^2 \end{pmatrix} = \underbrace{\frac{1}{2|T_{\bar{\mathbf{x}}\mathbf{x}_i^1\mathbf{x}_i^2}|} \begin{pmatrix} (\mathbf{x}_i^1-\mathbf{x}_i)^\perp \mathbf{K}(\mathbf{x}_i^2-\bar{\mathbf{x}})^\perp & (\mathbf{x}_i^1-\mathbf{x}_i)^\perp \mathbf{K}(\bar{\mathbf{x}}-\mathbf{x}_i^1)^\perp \\ (\mathbf{x}_i-\mathbf{x}_i^2)^\perp \mathbf{K}(\mathbf{x}_i^2-\bar{\mathbf{x}})^\perp & (\mathbf{x}_i-\mathbf{x}_i^2)^\perp \mathbf{K}(\bar{\mathbf{x}}-\mathbf{x}_i^1)^\perp \end{pmatrix}}_{G_i^A} \begin{pmatrix} \lambda_i^1 - P^A \\ \lambda_i^2 - P^A \end{pmatrix} \tag{29}$$

where $|T_{\bar{\mathbf{x}}\mathbf{x}_i^1\mathbf{x}_i^2}|$ is the area of the triangle spanned by the points $\bar{\mathbf{x}}$, $\mathbf{x}_i^1$ and $\mathbf{x}_i^2$ and, for example, the vector $(\mathbf{x}_i^1-\mathbf{x}_i)^\perp$ is obtained by a $\pi/2$ rotation of the vector $\mathbf{x}_i^1-\mathbf{x}_i$.

All subcells sharing vertex $\mathbf{x}_i$ create an interaction volume (see Figure 3).

The discretization is accomplished by assuming continuous fluxes across each of the subedges and a weak continuity condition of the pressure across the same edges. From these assumptions, an explicit discrete flux can be found after resolution of a local linear system and eliminating the edge pressure for each subedge of the interaction volume (see [19] for details). Each subedge flux can then be expressed explicitly as a weighted sum of the cell pressures of the interaction volume. For example, for Figure 3, we obtain

$$Q_i^1 = \sum_{k=1}^{5} t_i^k P^{A_k} \tag{30}$$

where t_i^k are transmissibility coefficients and A_k are located at the gravity centre of the triangles.

3.2. Localization of continuity points: Symmetric or non-symmetric MPFA formulations

The final system of MPFA is obtained by expressing the mass balance over each triangle: sum of the six subedge fluxes of the element equals the sink/source term over that element. The resulting mass matrix can be symmetric or non-symmetric depending on the localization of the continuity

DOI: 10.1002/fld

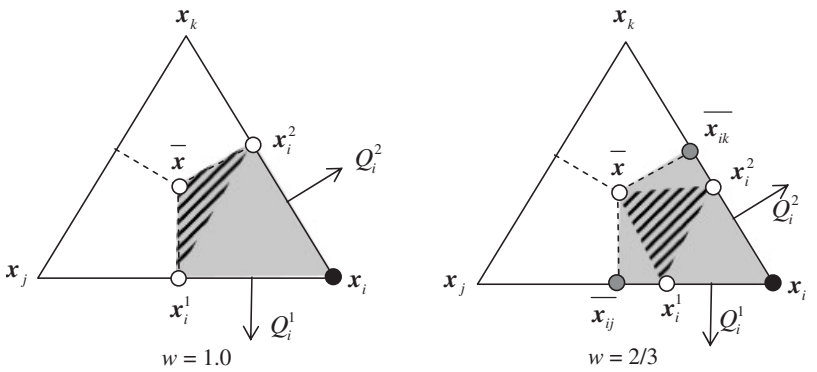

Figure 4. Two locations of the continuity point at the subcell interface. Local pressure support for $w=1.0$ and $\frac{2}{3}$.

points. Indeed, as shown in [17], symmetry of the global matrix is guaranteed only if this property is respected for each local matrix G_i^A.

On the other hand, continuity of the pressure is generally prescribed at the element-edge midpoint. This corresponds to $w=|\mathbf{x}_i^1-\mathbf{x}_i/\overline{\mathbf{x}_{ij}}-\mathbf{x}_i|=1$ with $\overline{\mathbf{x}_{ij}}=(\mathbf{x}_i+\mathbf{x}_j)/2$ (see Figure 4). In this case, the local matrix G_i^A in (29) is always non-symmetric.

However, as shown in [30], there is flexibility in the location of the continuity point. Its position can be chosen to lie at any point between the edge midpoint and the vertex (Figure 4).

The symmetry is achieved when the continuity point is localized at $w=\frac{2}{3}$ (Figure 4). In this case, $\mathbf{x}_i^1, \mathbf{x}_i, \mathbf{x}_i^2, \bar{\mathbf{x}}$ is a parallelogram and the local matrix G_i^A in the half-edge fluxes expression (29) becomes

$$Gs_i^A=\frac{1}{2|T_{\bar{\mathbf{x}}\mathbf{x}_i^1\mathbf{x}_i^2}|}\begin{pmatrix}(\overline{\mathbf{x}_{ij}}-\mathbf{x}_i)^\perp\mathbf{K}(\mathbf{x}_i^2-\bar{\mathbf{x}})^\perp & (\overline{\mathbf{x}_{ij}}-\mathbf{x}_i)^\perp\mathbf{K}(\bar{\mathbf{x}}-\mathbf{x}_i^1)^\perp\\ (\mathbf{x}_i-\overline{\mathbf{x}_{ik}})^\perp\mathbf{K}(\mathbf{x}_i^2-\bar{\mathbf{x}})^\perp & (\mathbf{x}_i-\overline{\mathbf{x}_{ik}})^\perp\mathbf{K}(\bar{\mathbf{x}}-\mathbf{x}_i^1)^\perp\end{pmatrix} \tag{31}$$

which can be shown to be symmetric when replacing $\bar{\mathbf{x}}=(\mathbf{x}_i+\mathbf{x}_j+\mathbf{x}_k)/3$, $\overline{\mathbf{x}_{ij}}=(\mathbf{x}_i+\mathbf{x}_j)/2$, $\overline{\mathbf{x}_{ik}}=(\mathbf{x}_i+\mathbf{x}_k)/2$, $\mathbf{x}_i^1=\mathbf{x}_i/3+2\overline{\mathbf{x}_{ij}}/3$ and $\mathbf{x}_i^2=\mathbf{x}_i/3+2\overline{\mathbf{x}_{ik}}/3$.

Therefore, one can obtain a symmetric MPFA formulation for general triangular elements without any approximate numerical integration. Recall that for quadrilateral grids, the MPFA method leads to a symmetric matrix only in the case of parallelograms (constant Jacobian). For quadrilateral elements, numerical quadrature allows the formulation of a symmetric MPFA formulation which, has similar convergence behaviour as the standard formulation for h^2-perturbed parallelograms [22, 23, 26]. However, a loss of convergence has been observed for the symmetric MPFA formulation on rough grids [23, 26].

4. THE MPFA FORMULATION OF RT0 AND BDM1

In this section, we show, algebraically, the link between hybrid and MPFA formulations of both RT0 and BDM1 mixed methods.

DOI: 10.1002/fld

4.1. The MPFA formulation of RT0

In the case of triangles, the inverse of the elemental matrix B, defined by (15), gives [16]

$$[B]^{-1}=\frac{\det(\mathbf{K})}{|A|}\begin{bmatrix}\mathbf{x}_{ij}\mathbf{K}^{-1}\mathbf{x}_{ij} & \mathbf{x}_{ij}\mathbf{K}^{-1}\mathbf{x}_{ki} & \mathbf{x}_{ij}\mathbf{K}^{-1}\mathbf{x}_{jk}\\ \mathbf{x}_{ki}\mathbf{K}^{-1}\mathbf{x}_{ij} & \mathbf{x}_{ki}\mathbf{K}^{-1}\mathbf{x}_{ki} & \mathbf{x}_{ki}\mathbf{K}^{-1}\mathbf{x}_{jk}\\ \mathbf{x}_{jk}\mathbf{K}^{-1}\mathbf{x}_{ij} & \mathbf{x}_{jk}\mathbf{K}^{-1}\mathbf{x}_{ki} & \mathbf{x}_{jk}\mathbf{K}^{-1}\mathbf{x}_{jk}\end{bmatrix}+\frac{1}{3\ell}\begin{bmatrix}1 & 1 & 1\\ 1 & 1 & 1\\ 1 & 1 & 1\end{bmatrix} \tag{32}$$

The dimensionless shape coefficient ℓ is defined by [6]

$$\ell=\sum_{j=1}^{3}B_{ij} \tag{33}$$

Equation (18) becomes

$$P^A=\left(\frac{TP_1^A+TP_2^A+TP_3^A}{3}\right)+\frac{\ell}{3}Q_s^A \tag{34}$$

Recall that the fluxes across edges are given by

$$Q_i^A=\sum_{k=1}^{3}B_{i,k}^{-1}(P^A-TP_k^A) \tag{35}$$

The expression of TP_3^A is obtained from (34) and is then replaced in (35). The substitution of (32) into (35) gives the fluxes across the two first edges:

$$\begin{aligned}\begin{pmatrix}Q_1^A\\ Q_2^A\end{pmatrix}=&\frac{\det(\mathbf{K})}{|A|}\begin{pmatrix}\mathbf{x}_{12}\mathbf{K}^{-1}(\mathbf{x}_{23}-\mathbf{x}_{12}) & \mathbf{x}_{12}\mathbf{K}^{-1}(\mathbf{x}_{23}-\mathbf{x}_{31})\\ \mathbf{x}_{31}\mathbf{K}^{-1}(\mathbf{x}_{23}-\mathbf{x}_{12}) & \mathbf{x}_{31}\mathbf{K}^{-1}(\mathbf{x}_{23}-\mathbf{x}_{31})\end{pmatrix}\begin{pmatrix}(TP_1^A-P^A)\\ (TP_2^A-P^A)\end{pmatrix}\\ &+Q_s^A\begin{pmatrix}\dfrac{\det(\mathbf{K})}{|A|}(\mathbf{x}_{12}\mathbf{K}^{-1}\mathbf{x}_{23})\ell+\dfrac{1}{3}\\ \dfrac{\det(\mathbf{K})}{|A|}(\mathbf{x}_{32}\mathbf{K}^{-1}\mathbf{x}_{23})\ell+\dfrac{1}{3}\end{pmatrix}\end{aligned} \tag{36}$$

Using the following properties on triangles:

$$\begin{aligned}\frac{\det(\mathbf{K})}{|A|}\mathbf{x}_{ij}\mathbf{K}^{-1}(\mathbf{x}_{jk}-\mathbf{x}_{ij})&=\frac{1}{4|T_{\bar{\mathbf{x}}\mathbf{x}_i^1\mathbf{x}_i^2}|}(\mathbf{x}_i^1-\mathbf{x}_i)^{\perp}\mathbf{K}(\mathbf{x}_i^2-\bar{\mathbf{x}})^{\perp}\\ \frac{\det(\mathbf{K})}{|A|}\mathbf{x}_{ij}\mathbf{K}^{-1}(\mathbf{x}_{jk}-\mathbf{x}_{ki})&=\frac{1}{4|T_{\bar{\mathbf{x}}\mathbf{x}_i^1\mathbf{x}_i^2}|}(\mathbf{x}_i^1-\mathbf{x}_i)^{\perp}\mathbf{K}(\bar{\mathbf{x}}-\mathbf{x}_i^1)^{\perp}\end{aligned} \tag{37}$$

DOI: 10.1002/fld

the fluxes (36) with RT0 become

$$\begin{pmatrix} Q_1^A \\ Q_2^A \end{pmatrix} = \frac{1}{4|T_{\bar{\mathbf{x}}\mathbf{x}_1^1\mathbf{x}_1^2}|} \begin{pmatrix} (\mathbf{x}_1^1-\mathbf{x}_1)^\perp \mathbf{K}(\mathbf{x}_1^2-\bar{\mathbf{x}})^\perp & (\mathbf{x}_1^1-\mathbf{x}_1)^\perp \mathbf{K}(\bar{\mathbf{x}}-\mathbf{x}_1^1)^\perp \\ (\mathbf{x}_1-\mathbf{x}_1^2)^\perp \mathbf{K}(\mathbf{x}_1^2-\bar{\mathbf{x}})^\perp & (\mathbf{x}_1-\mathbf{x}_1^2)^\perp \mathbf{K}(\bar{\mathbf{x}}-\mathbf{x}_1^1)^\perp \end{pmatrix} \begin{pmatrix} (TP_1^A - P^A) \\ (TP_2^A - P^A) \end{pmatrix}$$
$$+ Q_s^A \begin{pmatrix} \dfrac{\det(\mathbf{K})}{|A|}(\mathbf{x}_{12}\mathbf{K}^{-1}\mathbf{x}_{23})\ell + \dfrac{1}{3} \\ \dfrac{\det(\mathbf{K})}{|A|}(\mathbf{x}_{32}\mathbf{K}^{-1}\mathbf{x}_{23})\ell + \dfrac{1}{3} \end{pmatrix} \tag{38}$$

Therefore, half-edge fluxes can be expressed in the following form:

$$\begin{pmatrix} Q_1^1 \\ Q_1^2 \end{pmatrix} = [G_1^A] \begin{pmatrix} \lambda_1^1 - P^A \\ \lambda_1^2 - P^A \end{pmatrix} + \begin{pmatrix} Qs_1^1 \\ Qs_1^2 \end{pmatrix} \tag{39}$$

where $[G_1^A]$ is given by (29), $Q_1^1 = Q_1^A/2$, $Q_1^2 = Q_2^A/2$, $\lambda_1^1 = TP_1^A$, $\lambda_1^2 = TP_2^A$ and

$$\begin{pmatrix} Qs_1^1 \\ Qs_1^2 \end{pmatrix} = \begin{pmatrix} \dfrac{\det(\mathbf{K})}{2|A|}(\mathbf{x}_{12}\mathbf{K}^{-1}\mathbf{x}_{23})\, Q_s^A \ell + \dfrac{Q_s^A}{6} \\ \dfrac{\det(\mathbf{K})}{2|A|}(\mathbf{x}_{31}\mathbf{K}^{-1}\mathbf{x}_{23})\, Q_s^A \ell + \dfrac{Q_s^A}{6} \end{pmatrix} \tag{40}$$

Therefore, the MPFA formulation of the lowest RT0 mixed method can be obtained by (i) using (29) on the interaction volume (Figure 3) instead of (29) and (ii) assuming continuity of fluxes and pressure across the subedges of the interaction volume.

Contrary to the standard MPFA method, each subedge flux is now expressed explicitly as a weighted sum of not only the cell pressures but also the cell sink/source terms of the elements in the interaction volume. For example, for Figure 3 we obtain

$$Q_i^1 = \sum_{k=1}^{5} t_i^k P^{A_k} + \sum_{k=1}^{5} \gamma_i^k Qs^{A_k} \tag{41}$$

The final system for the MPFA formulation of the RT0 MFE method is then obtained when the mass balance is expressed over each triangle. This MPFA formulation is equivalent to the mixed hybrid formulation, and this without any numerical integration [21]. In the case of steady-state flow without sink/source terms, (39) reduces to (29) and the MPFA mixed formulation of RT0 is algebraically equivalent to the standard MPFA method.

4.2. The MPFA formulation of BDM1

Contrary to RT0, numerical integration is required to construct the MPFA formulation of BDM1. To this aim, the local matrix $[B]$, given in (25), is evaluated using the following quadrature rule [3, 24]:

$$B_{i,j,k,l} = \int_{\widehat{A}} \widehat{\boldsymbol{\omega}}_{i,j}^{\mathrm{BDM1,T}} \widehat{\mathbf{K}}^{-1} \widehat{\boldsymbol{\omega}}_{k,l}^{\mathrm{BDM1}} \simeq \frac{|\widehat{A}|}{3} [(\widehat{\boldsymbol{\omega}}_{i,j}^{\mathrm{BDM1,T}} \widehat{\mathbf{K}}^{-1} \widehat{\boldsymbol{\omega}}_{k,l}^{\mathrm{BDM1}})_{(0,0)} + (\widehat{\boldsymbol{\omega}}_{i,j}^{\mathrm{BDM1,T}} \widehat{\mathbf{K}}^{-1} \widehat{\boldsymbol{\omega}}_{k,l}^{\mathrm{BDM1}})_{(1,0)}$$
$$+ (\widehat{\boldsymbol{\omega}}_{i,j}^{\mathrm{BDM1,T}} \widehat{\mathbf{K}}^{-1} \widehat{\boldsymbol{\omega}}_{k,l}^{\mathrm{BDM1}})_{(0,1)}] \tag{42}$$

DOI: 10.1002/fld

Recall that from (9), we have on the edge A_l with the two end points (vertices) $\mathbf{r}_{lk}$ $(k=1,2)$,

$$\widehat{\boldsymbol{\omega}}_{i,j}^{\mathrm{BDM1}}(\mathbf{r}_{lk})\mathbf{n}_{A_l}=2\delta_{il}\delta_{jk} \quad \text{for } l=1,\ldots,3 \text{ and } k=1,2 \tag{43}$$

Therefore, using (42) and (43) to compute the local matrix $[B]$ gives a block-diagonal matrix where only the two vectorial basis functions associated with a corner $\widehat{x_i}$ are coupled. The (6×6) linear system (26) reduces to three (2×2) linear systems (one for each vertex). For example, for vertex 1 of coordinates $(0,0)$ in Figure 3, only $\widehat{\boldsymbol{\omega}}_{1,1}^{\mathrm{BDM1}}$ and $\widehat{\boldsymbol{\omega}}_{2,1}^{\mathrm{BDM1}}$ are non-zero and the corresponding (2×2) local system is

$$\frac{1}{6}\begin{pmatrix}(\widehat{\boldsymbol{\omega}}_{1,1}^{\mathrm{BDM1,T}}\widehat{\mathbf{K}}^{-1}\widehat{\boldsymbol{\omega}}_{1,1}^{\mathrm{BDM1}})_{(0,0)} & (\widehat{\boldsymbol{\omega}}_{1,1}^{\mathrm{BDM1,T}}\widehat{\mathbf{K}}^{-1}\widehat{\boldsymbol{\omega}}_{2,1}^{\mathrm{BDM1}})_{(0,0)}\\ (\widehat{\boldsymbol{\omega}}_{1,1}^{\mathrm{BDM1,T}}\widehat{\mathbf{K}}^{-1}\widehat{\boldsymbol{\omega}}_{2,1}^{\mathrm{BDM1}})_{(0,0)} & (\widehat{\boldsymbol{\omega}}_{2,1}^{\mathrm{BDM1,T}}\widehat{\mathbf{K}}^{-1}\widehat{\boldsymbol{\omega}}_{2,1}^{\mathrm{BDM1}})_{(0,0)}\end{pmatrix}\begin{pmatrix}Q_{1,1}^{A}\\ Q_{2,1}^{A}\end{pmatrix}=\begin{pmatrix}P^{A}-TP_{1,1}^{A}\\ P^{A}-TP_{2,1}^{A}\end{pmatrix} \tag{44}$$

Substituting expressions of $\widehat{\boldsymbol{\omega}}_{1,1}^{\mathrm{BDM1}}$ and $\widehat{\boldsymbol{\omega}}_{2,1}^{\mathrm{BDM1}}$ from Table I in (44) and inverting the obtained local system leads to the following formulation:

$$\begin{pmatrix}Q_i^1\\ Q_i^2\end{pmatrix}=[Gs_i^A]\begin{pmatrix}\lambda_i^1-P^A\\ \lambda_i^2-P^A\end{pmatrix} \tag{45}$$

where $[Gs_i^A]$ is the local matrix given in (31) and $Q_i^1=Q_{1,1}^A$, $Q_i^2=Q_{2,1}^A$, $\lambda_i^1=TP_{1,1}^A$, $\lambda_i^2=TP_{2,1}^A$.

Therefore, this system is equivalent to the symmetric MPFA system obtained when the continuity point is localized at $w=\frac{2}{3}$ (Figure 4).

In conclusion, the MPFA formulation of the BDM1 mixed method on triangles is obtained by using a special quadrature rule that reduces the BDM1 method to the symmetric MPFA method.

5. EFFICIENCY OF HYBRID AND MIXED FORMULATIONS OF RT0 AND BDM1

This section is devoted to the numerical efficiency and accuracy of the four mixed formulations (Hybrid_RT0, MPFA_RT0, Hybrid_BDM1 and MPFA_BDM1) on high anisotropic and heterogeneous media with unstructured triangular discretizations.

Properties of the four mixed formulations are summarized in Table II. It is clear from this table that the MPFA_RT0 is the less efficient formulation. This formulation is generally avoided for very large systems. Indeed, this formulation does not lead to a symmetric positive-definite matrix for general problems. Consequently, the obtained system cannot be solved with standard iterative solvers based on the conjugate gradient method.

Table II. Properties of Hybrid_RT0, MPFA_RT0, Hybrid_BDM1 and MPFA_BDM1 formulations.

	Hybrid_RT0	MPFA_RT0	Hybrid_BDM1	MPFA_BDM1
Numerical quadrature	No	No	No	Yes
Symmetric and positive-definite matrix	Yes	No	Yes	Yes
Number of unknowns	Nbr-edges	Nbr-elements	$2\times$Nbr-edges	Nbr-elements
Stencil	5	≈ 15	10	≈ 15

DOI: 10.1002/fld

The MPFA_RT0 formulation is therefore excluded, and the rest of the paper is devoted to the numerical efficiency of the three formulations: Hybrid_RT0, Hybrid_BDM1 and MPFA_BDM1. These three formulations give symmetric positive-definite matrix systems.

5.1. Numerical experiments

We define a test problem to study the efficiency of mixed formulations. The system (1) is solved on a unit square shape $\Omega=(0,1)^2$ domain with anisotropic and heterogeneous permeability field. The tensor coefficient and the true solution for the test problem are similar to the test problem given in [31]

$$K=\begin{bmatrix} y^2+\alpha x^2 & (\alpha-1)xy \\ (\alpha-1)xy & x^2+\alpha y^2 \end{bmatrix} \tag{46}$$

$$P(x,y)=\exp\left(-20\pi\left(\left(x-\frac{1}{2}\right)^2+\left(y-\frac{1}{2}\right)^2\right)\right) \tag{47}$$

The behaviours of all formulations are studied numerically for different anisotropies and different triangular discretizations.

For practical test cases, a high accuracy for the velocity field is often required (as, for example, for the simulation of transport of contaminant). The velocity error is investigated in the discrete L^2-norm defined by

$$\mathrm{ev}_{L^2}=\left(\sum_i |A_i|(\mathbf{q}_{\mathrm{an},i}-\mathbf{q}_i)^2 \Big/ \sum_i |A_i|\right)^{1/2} \tag{48}$$

where $|A_i|$ is the area of element i and $\mathbf{q}_{\mathrm{an},i}$ the analytical velocity evaluated at the centre of i obtained by the derivation of (47).

5.1.1. The isotropic case on structured meshes. The test problem is first solved for the isotropic case ($\alpha=1$) with different meshes. The first level of refinement is obtained from a discretization of a (25×25) square. The triangulation is obtained by subdivision of each square into four equal triangles by joining the centre of the square to its vertices. Finer discretizations are obtained starting from grids of (50×50), (100×100) and (200×200) squares. Table III gives results with the Hybrid_RT0, Hybrid_BDM1 and MPFA_BDM1 formulations for different levels of mesh refinement.

The linear system obtained by the three formulations is solved with the iterative preconditioned conjugate gradient solver. This solver is efficient and largely used in numerical codes. In this work, the solver is preconditioned with the Eisenstat procedure [32] and the tolerance is fixed to 10^{-16}. The total number of unknowns N_{unk}, the number of iterations N_{it} required by the solver to reach the convergence , the central processing unit (CPU) time t_{CPU} and velocity error are given in Table III.

Results of this table show that

- The CPU cost of the MPFA_BDM1 and Hybrid_RT0 are very close, especially for fine meshes. This is due to the fact that MPFA_BDM1 formulation has less unknowns but with a wider stencil than Hybrid_RT0 formulation.

DOI: 10.1002/fld

Table III. Results of Hybrid_RT0, Hybrid_BDM1 and MPFA_BDM1 for different mesh refinements.

	Mesh 1			Mesh 2			Mesh 3			Mesh 4		
	Hybrid_ RT0	Hybrid_ BDM1	MPFA_ BDM1	Hybrid_ RT0	Hybrid_ BDM1	MPFA_ BDM1	Hybrid_ RT0	Hybrid_ BDM1	MPFA_ BDM1	Hybrid_ RT0	Hybrid_ BDM1	MPFA_ BDM1
N_{unk}	3800	7600	2500	15 100	30 200	10 000	60 200	120 400	40 000	240 400	280 800	160 000
N_{it}	142	269	100	276	527	194	544	1033	380	1153	2057	760
t_{CPU}	0.05	0.14	0.08	0.27	1.03	0.45	2.2	12.6	3.1	25.7	110	24.5
ev_{L^2}	$7.8\times$ 10^{-2}	$2.5\times$ 10^{-2}	$4.7\times$ 10^{-2}	$3.95\times$ 10^{-2}	$1.07\times$ 10^{-2}	$2.27\times$ 10^{-2}	$2.0\times$ 10^{-2}	$7.2\times$ 10^{-3}	$1.2\times$ 10^{-2}	$1.15\times$ 10^{-2}	$6.3\times$ 10^{-3}	$8.1\times$ 10^{-3}

DOI: 10.1002/fld

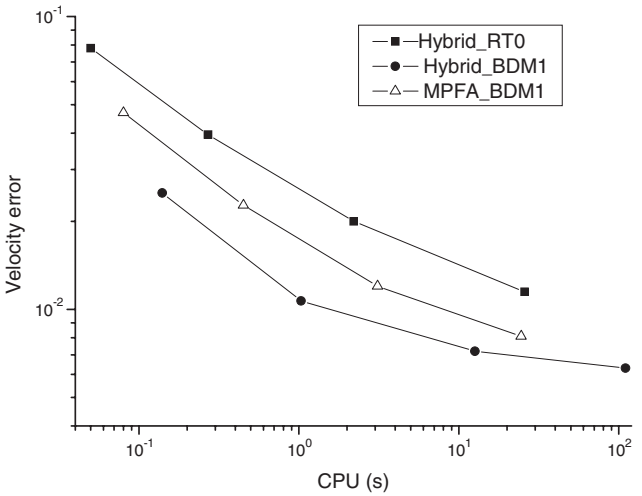

Figure 5. Velocity errors with Hybrid-RT0, Hybrid_BDM1 and MPFA_BDM1 for different meshes.

- The Hybrid_BDM1 formulation requires less CPU time than Hybrid_RT0 to achieve a fixed velocity accuracy (Figure 5).
- In the case of structured mesh and isotropic domain, the MPFA_BDM1 gives more accurate results than Hybrid_RT0 but less than Hybrid_BDM1.

5.1.2. Effects of anisotropy. The test problem is now simulated with different anisotropy factors and uses the coarser discretization described above.

Results of simulations, given in Table IV, show that

- The number of iterations and the CPU time increase when α increases for the three formulations.
- For anisotropic domains, the pressure solution presents non-physical oscillations (negative values). These oscillations are much more pronounced with Hybrid_RT0 than with Hybrid_BDM1 or MPFA_BDM1.
- The CPU time of MPFA_BDM1 becomes very close to the CPU time of Hybrid_RT0 when α increases (Figure 6).
- The velocity error of the three formulations is highly dependent on the anisotropy factor (Figure 7).
- When α increases, the velocity error of MPFA_BDM1 becomes very close to Hybrid_BDM1 error. However, MPFA_BDM1 requires four times less CPU time than Hybrid_BDM1.

These results show that MPFA_BDM1 is well suited for high anisotropic domains since it has the accuracy of Hybrid_BDM1 and the rapidity of Hybrid_RT0.

5.1.3. Effects of mesh distortion. Mesh distortion can have an important effect on the solution of the numerical method. For example, it was shown in [23, 26] that on rough quadrilateral grids, a loss of convergence can be observed for the MPFA_BDM1 formulation. In this section, we study

DOI: 10.1002/fld

Table IV. Results of Hybrid_RT0, Hybrid_BDM1 and MPFA_BDM1 for different anisotropy factors.

	$\alpha=1$			$\alpha=10$			$\alpha=100$			$\alpha=1000$		
	Hybrid_ RT0	Hybrid_ BDM1	MPFA_ BDM1	Hybrid_ RT0	Hybrid_ BDM1	MPFA_ BDM1	Hybrid_ RT0	Hybrid_ BDM1	MPFA_ BDM1	Hybrid_ RT0	Hybrid_ BDM1	MPFA_ BDM1
N_{it}	142	269	100	209	338	121	326	472	179	627	549	240
t_{CPU}	4.7×10^{-2}	0.14	7.8×10^{-2}	6.3×10^{-2}	0.17	9.3×10^{-2}	7.8×10^{-2}	0.23	0.1	0.125	0.25	0.12
P_{Min}	-1.9×10^{-4}	-8.5×10^{-5}	-5.1×10^{-5}	-5.4×10^{-4}	-4.1×10^{-4}	-1.2×10^{-4}	−0.22	-1.5×10^{-3}	-3.8×10^{-3}	−3.43	-3×10^{-2}	−0.1
P_{Max}	0.98	0.98	0.99	1.06	0.98	0.99	1.81	0.99	1.001	8.76	1.2	1.1
ep_{L^2}	6.3×10^{-4}	1.9×10^{-3}	8×10^{-4}	4.6×10^{-3}	1.8×10^{-3}	1.2×10^{-3}	5.6×10^{-2}	1.6×10^{-3}	2.9×10^{-3}	0.52	9.3×10^{-3}	2.6×10^{-2}
ev_{L^2}	7.9×10^{-2}	2.5×10^{-2}	4.6×10^{-2}	0.65	0.18	0.24	6.7	2.1	2.44	67.3	28.6	27

DOI: 10.1002/fld

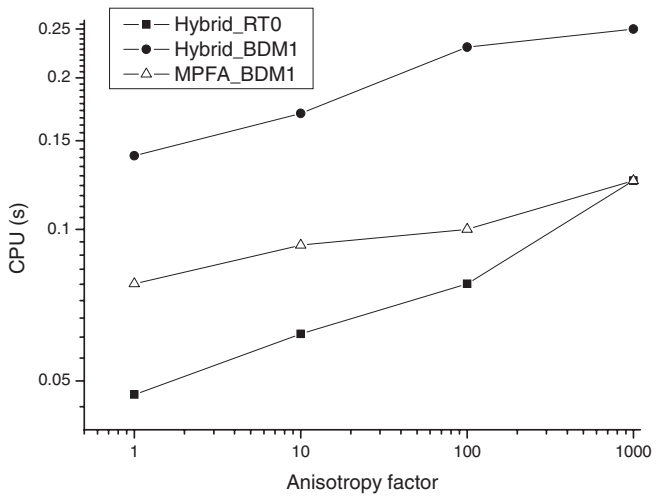

Figure 6. CPU time with Hybrid_RT0, Hybrid_BDM1 and MPFA_BDM1 for different anisotropy factors.

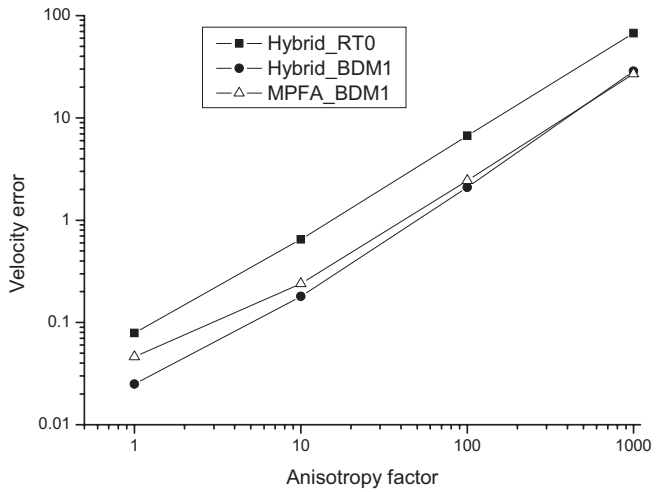

Figure 7. Velocity errors with Hybrid_RT0, Hybrid_BDM1 and MPFA_BDM1 for different anisotropy factors.

this effect on the behaviour of the solution of Hybrid_RT0, Hybrid_BDM1 and MPFA_BDM1 formulations.

The previous triangulations are obtained from subdivision of squares. To obtain a highly unstructured triangulation, the centre of each square is moved randomly inside the square. Four different triangles are obtained by joining this point to the vertices of the square.

This procedure is performed at each level of refinement. Figure 8 shows the unstructured triangular mesh obtained from the coarser discretization.

DOI: 10.1002/fld

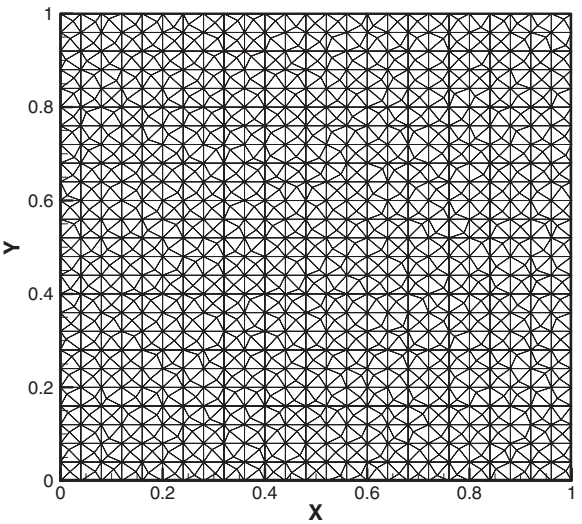

Figure 8. Unstructured triangulation obtained from randomly moving the centre of squares.

Results for different unstructured meshes with a coefficient of anisotropy of $\alpha = 50$ are given in Table V and Figures 9 and 10. These results show that

- The symmetric MPFA formulation on triangles is highly efficient on unstructured meshes and MPFA_BDM1 results are not deteriorated on unstructured meshes.
- The Hybrid_RT0 gives less stable pressure results than Hybrid_BDM1 and MPFA_BDM1. The maximum pressure value with Hybrid_RT0 is greater than 1 for all meshes.
- Concerning pressure errors, MPFA_BDM1 is the more efficient method. Indeed, for a given pressure error of 5×10^{-4}, MPFA_BDM1 spends 20 times less CPU time than Hybrid_RT0 and four times less than Hybrid_BDM1 (Figure 9).
- Similar performances are obtained for MPFA_BDM1 concerning velocity errors. Indeed, MPFA_BDM1 can spend 10 times less CPU time than Hybrid_RT0 and three times less than Hybrid_BDM1 for a given velocity error (Figure 10).

These results show that the MPFA_BDM1 formulation outperforms both Hybrid_RT0 and Hybrid_BDM1 formulations for anisotropic domains and unstructured triangular meshes.

6. CONCLUSION

In this paper, hybrid and MPFA formulations of both RT0 and BDM1 mixed methods were developed. The link between these formulations was shown algebraically for RT0 and BDM1 on triangular meshes.

The MPFA_RT0 formulation is obtained without any numerical integration from the mixed formulation. Whereas, the MPFA_BDM1 formulation is obtained by using a special quadrature rule that reduces the BDM1 method to the symmetric MPFA method.

DOI: 10.1002/fld

Table V. Results of Hybrid_RT0, Hybrid_BDM1 and MPFA_BDM1 for different unstructured meshes and $\alpha = 50$.

	Mesh 1			Mesh 2			Mesh 3			Mesh 4		
	Hybrid_ RT0	Hybrid_ BDM1	MPFA_ BDM1	Hybrid_ RT0	Hybrid_ BDM1	MPFA_ BDM1	Hybrid_ RT0	Hybrid_ BDM1	MPFA_ BDM1	Hybrid_ RT0	Hybrid_ BDM1	MPFA_ BDM1
N_{unk}	3800	7600	2500	15 100	30 200	10 000	60 200	120 400	40 000	240 400	280 800	160 000
N_{it}	305	453	164	590	901	323	1155	1788	646	2286	3551	1275
t_{CPU}	0.06	0.22	0.1	0.5	1.75	0.59	4.25	21.5	4.7	50.3	188.9	38.9
P_{Min}	$-7.7\times$ 10^{-2}	$-1.6\times$ 10^{-3}	$-4.0\times$ 10^{-3}	$-6.4\times$ 10^{-3}	$-3.9\times$ 10^{-4}	$-8.5\times$ 10^{-4}	$-6.8\times$ 10^{-4}	$-8.5\times$ 10^{-5}	$-1.8\times$ 10^{-4}	$-2.1\times$ 10^{-4}	$-2.1\times$ 10^{-5}	$-4.8\times$ 10^{-5}
P_{Max}	1.4	0.98	1.007	1.1	0.99	0.997	1.03	0.999	0.999	1.01	0.999	0.999
ep_{L^2}	$3.1\times$ 10^{-2}	$1.8\times$ 10^{-3}	$2.8\times$ 10^{-3}	$7.8\times$ 10^{-3}	$4.6\times$ 10^{-4}	$6.3\times$ 10^{-4}	$1.94\times$ 10^{-3}	$1.14\times$ 10^{-4}	$1.5\times$ 10^{-4}	$4.9\times$ 10^{-4}	$2.9\times$ 10^{-5}	$3.8\times$ 10^{-5}
ev_{L^2}	3.53	0.99	1.15	1.7	0.42	0.51	0.89	0.27	0.31	0.48	0.24	0.25

DOI: 10.1002/fld

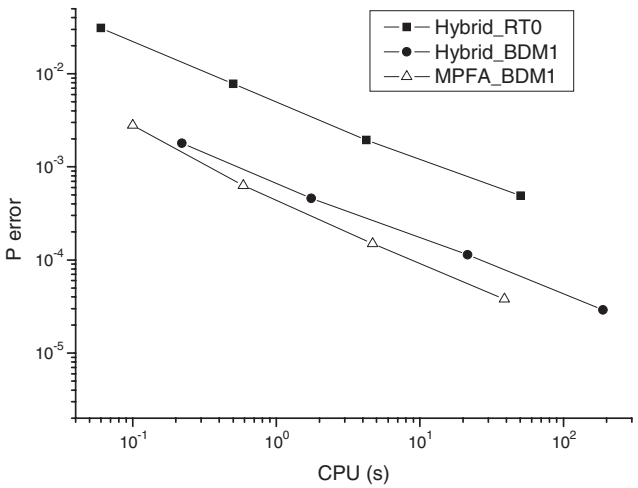

Figure 9. Pressure errors with Hybrid_RT0, Hybrid_BDM1 and MPFA_BDM1 on unstructured meshes.

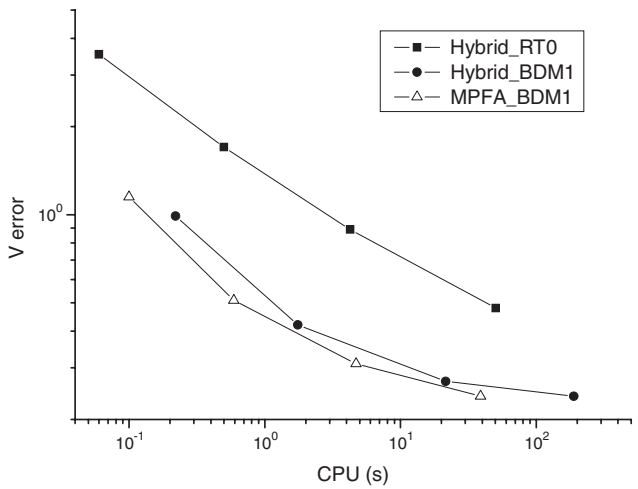

Figure 10. Velocity errors with Hybrid_RT0, Hybrid_BDM1 and MPFA_BDM1 on unstructured meshes.

Performance of the four mixed formulations (Hybrid_RT0, Hybrid_BDM1, MPFA_RT0 and MPFA_BDM1) was investigated on anisotropic and heterogeneous media with unstructured meshes.

The MPFA_RT0 is the less efficient formulation. It uses fewer unknowns than Hybrid_RT0 but the matrix of the discrete system is non-symmetric and is not positive definite.

Numerical experiments show that, in general, BDM1 formulations (Hybrid_BDM1 and MPFA_BDM1) require less CPU time than Hybrid_RT0 to achieve a fixed velocity accuracy. The accuracy of the MPFA_BDM1 formulation is not deteriorated for highly unstructured triangular meshes (contrarily to quadrilateral meshes where a loss of convergence can be encountered

DOI: 10.1002/fld

for rough grids). For highly anisotropic domains and unstructured meshes, the MPFA_BDM1 formulation outperforms both Hybrid_RT0 and Hybrid_BDM1 and appears to be the successful choice when a high accuracy for the velocity field is required.

REFERENCES

1. Durlofsky LJ. Accuracy of mixed and control volume finite element approximations to Darcy velocity and related quantities. *Water Resources Research* 1994; **21**:965–973.
2. Darlow BL, Ewing RE, Wheeler MF. Mixed finite element method for miscible displacement problems in porous media. *Society of Petroleum Engineers Journal* 1984; **24**:391–398.
3. Brezzi F, Fortin M. *Mixed and Hybrid Finite Element Methods*. Springer: New York, 1991.
4. Bergamaschi L, Mantica S, Saleri F. Mixed finite element approximation of Darcy's law in porous media. *Technical Report*, *CRS4*, Cagliari, Italy, 1994.
5. Mosé R, Siegel P, Ackerer P, Chavent G. Application of the mixed hybrid finite element approximation in a groundwater flow model: luxury or necessity? *Water Resources Research* 1994; **30**:3001–3012.
6. Younes A, Ackerer Ph, Mosé R, Chavent G. A new formulation of the mixed finite element method for solving elliptic and parabolic PDE with triangular elements. *Journal of Computational Physics* 1999; **149**:148–167.
7. Ackerer Ph, Younes A, Mosé R. Modeling variable density flow and solute transport in porous medium: 1. Numerical model and verification. *Transport in Porous Media* 1999; **35**:345–373.
8. Chavent G, Younes A, Ackerer Ph. On the finite volume reformulation of the mixed finite element method for elliptic and parabolic PDE on triangles. *Computer Methods in Applied Mechanics and Engineering* 2003; **192**:655–682.
9. Younes A, Ackerer P, Lehmann F. A new mass lumping scheme for the mixed hybrid finite element method. *International Journal for Numerical Methods in Engineering* 2006; **67**:89–107.
10. Chavent G, Jaffré J. *Mathematical Models and Finite Elements for Reservoir Simulation*. North-Holland: Amsterdam, 1986.
11. Roberts JE, Thomas JM. Finite elements methods (part 1). In *Mixed and Hybrid Methods*, Ciarlet PG, Lions JL (eds), vol. II. North-Holland: Amsterdam, 1989.
12. Russel TF, Wheeler MF. Finite element and finite difference methods for continuous flows in porous media. In *The Mathematics of Reservoir Simulation*, Ewing RE (ed.). SIAM: Philadelphia, PA, 1983.
13. Weiser A, Wheeler MF. On convergence of block-centered finite differences for elliptic problems. *SIAM Journal on Numerical Analysis* 1988; **25**:351–375.
14. Baranger J, Maitre JF, Oudin F. Application de la théorie des éléments finis mixtes à l'étude d'une classe de schémas aux volumes-différences finis pour les problèmes elliptiques. *Comptes Rendus de l'Academie des Sciences Paris*, *Série I* 1994; **319**:401–404.
15. Arbogast T, Kennan PT. Mixed finite element methods as finite difference methods for solving elliptic equations on triangular elements. *Technical Report 93-53*, Department of Computational and Applied Mathematics, Rice University, 1984.
16. Younes A, Ackerer P, Chavent G. From mixed finite elements to finite volumes for elliptic PDE in 2 and 3 dimensions. *International Journal for Numerical Methods in Engineering* 2004; **59**:365–388.
17. Aavatsmark I, Barkve T, Bøe Ø, Mannseth T. Discretization on non-orthogonal, curvilinear grids for multiphase flow. In *Proceedings of 4th European Conference on the Mathematics of Oil Recovery*, Christie MA, Farmer CL, Guillon O, Heinmann ZE (eds). Norway, 1994.
18. Edwards MG, Rogers CF. A flux continuous scheme for the full tensor pressure equation. *Proceedings of the 4th European Conference on the Mathematics of Oil Recovery*, Røros, 1994.
19. Aavatsmark I. An introduction to multipoint flux approximations for quadrilateral grids. *Journal of Computational Geosciences* 2002; **6**:404–432.
20. Edwards MG, Rogers CF. Finite volume discretization with imposed flux continuity for the general tensor pressure equation. *Journal of Computational Geosciences* 1998; **2**:259–290.
21. Vohralik M. Equivalence between lowest-order mixed finite element and multi-point finite volume methods on simplicial meshes. *Mathematical Modelling and Numerical Analysis* 2006; **40**:367–391.
22. Klausen RA, Winther R. Convergence of multipoint flux approximations on quadrilateral grids. *Numerical Methods for Partial Differential Equations* 2006; **22**:1438–1454.
23. Klausen RA, Winther R. Robust convergence of multi-point flux approximations on rough grids. *Numerische Mathematik* 2006; **104**:317–337.

DOI: 10.1002/fld

24. Wheeler MF, Yotov I. A cell-centered finite difference method on quadrilaterals. In *Compatible Spatial Discretizations*, Arnold DN, Bochev PB, Lehoucq RB, Nicolaides RA, Shashkov M (eds), IMA Vol. Ser., vol. 142. Springer: New York, 2006; 189–207.
25. Wheeler MF, Yotov I. A multipoint flux mixed finite element method. *SIAM Journal on Numerical Analysis* 2006; **44**:2082–2106.
26. Aavatsmark I, Eigestad G, Klausen RA, Wheeler MF, Yotov I. Convergence of a symmetric MPFA method on quadrilateral grids. *Technical Report TR-MATH 05-14*, Department of Mathematics, University of Pittsburgh, Pittsburgh, PA, 2005.
27. Fraeijs de Veubeke BX. Displacement and equilibrium models in the finite element method. In *Stress Analysis*, Zienkiewicz OC, Hollister G (eds). New York, 1965.
28. Brezzi F, Douglas Jr J, Marini LD. Two families of mixed finite elements for second order elliptic problems. *Numerische Mathematik* 1985; **47**:217–235.
29. Brezzi F, Fortin M, Marini LD. Piecewise constant pressures for Darcy law. In *Finite Elements Methods*: *1970 and Beyond*, Franca LP (ed.). CIMNE: Barcelona, 2004.
30. Pal M, Edwards MG, Lamb AR. Convergence study of a family of flux-continuous, finite-volume schemes for the general tensor pressure equation. *International Journal for Numerical Methods in Fluids* 2006; **51**:1177–1203.
31. Le Potier C. Schéma volumes finis pour des opérateurs de diffusion fortement anisotropes sur des maillages non structures. *Comptes Rendu Mathematique* 2005; **12**:921–926.
32. Eisenstat SC. Efficient implementation of a class of preconditioned conjugate gradient methods. *SIAM Journal on Scientific and Statistical Computing* 1981; **2**:1–4.

DOI: 10.1002/fld